

THE GENERALIZATION RIDGE: INFORMATION FLOW IN NATURAL LANGUAGE GENERATION

Ruidi Chang, Chunyuan Deng, Hanjie Chen

Department of Computer Science

Rice University

Houston, TX 77005, USA

{ruidi.chang, chunyuan.deng, hanjie}@rice.edu

ABSTRACT

Transformer-based language models have achieved state-of-the-art performance in natural language generation (NLG), yet their internal mechanisms for synthesizing task-relevant information remain insufficiently understood. While prior studies suggest that intermediate layers often yield more generalizable representations than final layers, how this generalization ability emerges and propagates across layers during training remains unclear. To address this gap, we propose InfoRidge, an information-theoretic framework, to characterize how predictive information—the mutual information between hidden representations and target outputs—varies across depth. Estimating this quantity enables us to trace the flow of task-relevant information throughout the model during training. Our experiments across various models and datasets reveal a consistent non-monotonic trend: predictive information peaks in upper-middle layers—forming a **generalization ridge**—before declining in final layers, reflecting a transition between generalization and memorization. To further investigate this phenomenon, we introduce residual scaling coefficients—trainable scalar parameters applied to each residual block—which serve as functional probes for assessing the relative importance of individual transformer layers. These coefficients reveal that, under distribution shift, models downweight final layers and increasingly rely on intermediate layers, highlighting their role in generalization. Together, these findings offer new insights into the internal mechanisms of transformers and underscore the critical role of intermediate layers in supporting generalization.

1 INTRODUCTION

Transformer-based language models generate text by predicting tokens autoregressively, and they have achieved remarkable performance across a wide range of natural-language uses (Vaswani et al., 2017; Dong et al., 2022). Nevertheless, we lack a rigorous understanding of how these models acquire and synthesize task-relevant information during training.

A growing body of research has shown that intermediate layers in deep neural networks often surpass final layers in terms of representational quality and generalization performance (Liu et al., 2019b; Voita et al., 2019; Ansuini et al., 2019; Ahrens et al., 2023; Uselis & Oh, 2025). In language models, intermediate layers often encode richer semantic and more robust features than final layers (Fan et al., 2024; Jin et al., 2024; Skean et al., 2025). However, questions still remain: *In NLG, how does information evolve across layers during training, and how are different layers of the network functionally organized to support generalization versus memorization?*

To investigate these questions, we propose *InfoRidge*, an information-theoretic framework, to analyze information flow in language models. Building on matrix-based mutual information estimation (Giraldo et al., 2014), our approach quantifies how predictive signals transform across layers during training. We center our analysis on two complementary quantities: *predictive information*, defined as the mutual information $I(Z_\ell; Y)$ between the hidden representation Z_ℓ at layer ℓ and the next-token label Y , reflecting how much task-relevant information is preserved; *incremental infor-*

information gain, denoted as $I(\Delta Z_\ell; Y)$, where ΔZ_ℓ is the residual changes between successive layer ℓ and $\ell - 1$, measuring the additional predictive information introduced by each transformer block.

Using *InfoRidge*, we uncover a non-monotonic trend: predictive information rises through the early and middle layers, peaks in the upper-middle layers, and then declines in the later layers. We name this phenomenon the **generalization ridge**, where the model encodes the more generalizable task-relevant information. This ridge marks a structural division of labor: intermediate layers concentrate generalizable features that transfer across distributions, while later layers increasingly specialize in task-specific memorization. Incremental information gain further shows that ridge layers introduce the largest increases in predictive information, marking them as key contributors to the emergence of the ridge. This analysis directly connects the information peak to generalizable behavior and clarifies how generalization and memorization are distributed across depth.

To further validate this interpretation, we introduce *residual scaling coefficients*—learnable scalar parameters β_ℓ applied to each residual block—while keeping all other model weights frozen, drawing inspiration from prior work on layer-wise adaptation (Liu et al., 2019a; Menghani et al., 2024). A higher β_ℓ value indicates greater reliance on the corresponding layer’s output during prediction. These coefficients act as functional probes, revealing how the model redistributes layer-wise importance under different data distribution. Under in-distribution training, deeper layers retain higher residual weights, reflecting the model’s reliance on memorized, task-specific features. When evaluated under distribution shift, models have lower reliance on the final layer and shifts importance toward the intermediate layers.

To understand the formation of the generalization ridge, we analyze both attention patterns and model capacity. Attention analysis shows ridge layers attend to tokens that capture broadly useful features, aligning with the information peak. Beyond attention patterns, we also investigate the conditions under which the ridge emerges. Our depth ablation results show that the ridge only emerges beyond a certain depth threshold. Below this threshold, predictive information increases monotonically, indicating that sufficient capacity is a prerequisite for generalization ridge to emerge.

Contributions. Our work provides a unified perspective on how predictive information is structured across depth in transformer-based language models for natural language generation tasks:

1. Our work tracks the evolution of predictive information throughout training, establishing a clear connection between predictive information flow and generalization. It reveals a non-monotonic peak in the middle layers, which we refer to as the **generalization ridge**. This pattern reflects a meaningful transition in representational focus and aligns with stronger generalization behavior.
2. We introduce *InfoRidge*, an information-theoretic framework that applies matrix-based mutual information estimation to autoregressive language models to analyze information flow.
3. We introduce residual scaling coefficients as trainable indicators of how models shift representational focus across layers during training, providing a causal, adaptive measure of model behavior under distribution shifts.

2 RELATED WORK

Understanding how information is encoded and transformed across layers has been studied through probing classifiers (Alain & Bengio, 2016), attention flow (Vig & Belinkov, 2019), and information-theoretic approaches such as the information bottleneck (Shwartz-Ziv & Tishby, 2017), mutual information estimation (Goldfeld, 2019), and matrix-based entropy (Giraldo et al., 2014), offering different lenses to quantify representational capacity, abstraction, and invariance across layers.

A growing body of research has shown that intermediate layers in deep networks often outperform final layers in terms of representational quality and task performance (Ansuini et al., 2019; Yosinski et al., 2014; Uselis & Oh, 2025; Ahrens et al., 2023; Ando et al., 2023). In language models, mid-depth layers tend to capture richer semantic or robust features than output layers (Liu et al., 2019b; Voita et al., 2019; Jin et al., 2024; Fan et al., 2024). Transformer representations have long been observed to follow a structured progression from syntactic to semantic information, as shown by classical probing studies on linguistic knowledge and the reconstruction of the NLP pipeline (Liu

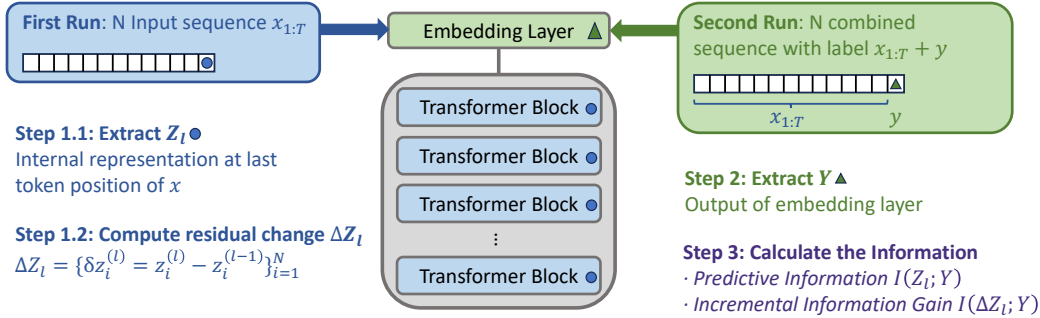


Figure 1: Overview of InfoRidge. (1) Step 1: Extract internal representations at each layer and compute residual changes between successive layers. (2) Step 2: Extract the target token embedding. (3) Step 3: Using these representations, we estimate the layer-wise predictive information $I(Z_\ell; Y)$ and the incremental information gain $I(\Delta Z_\ell; Y)$, which jointly characterize how information evolves across depth.

et al., 2019b; Tenney et al., 2019). These findings challenge the assumption that deeper layers always yield better representations.

This pattern holds across settings such as transfer learning (Yosinski et al., 2014), continual learning (Ahrens et al., 2023), and out-of-distribution generalization (Uselis & Oh, 2025). Furthermore, recent work has evaluated representation quality using entropy, curvature, and invariance (Skean et al., 2025), while other studies have examined embedding drift and representational geometry (Merchant et al., 2020; Dar et al., 2022), analyzed memorization and factual recall (Haviv et al., 2022; Yu et al., 2023), and introduced causal perspectives on layer importance through mediation analysis and targeted interventions (Vig et al., 2020; Meng et al., 2022). Training-dynamics studies investigated how earlier models develop and refine semantic features across depth, providing an additional perspective on the evolution of layer-wise representations (Merchant et al., 2020; Kumar et al., 2023). Correlational probes (e.g., linear probes (Alain & Bengio, 2016)) measure only whether a feature can be decoded from a representation, which reflects correlation but not causal influence. In contrast, causal methods intervene on internal activations to test how changing a component alters the model’s prediction, thereby identifying true causal contribution rather than mere feature presence. Our residual-scaling approach aligns with this causal perspective at the layer level.

However, the underlying causes and functional role of this phenomenon remain only partially understood, motivating further investigation. Our work addresses this gap by tracing the evolution of predictive information throughout training and establishing a clear connection between predictive information flow and generalization. We reveal a consistent non-monotonic peak in the middle layers—termed the *generalization ridge*—that reflects a meaningful transition in representational focus and aligns with stronger generalization behavior. Additionally, unlike prior work focused on classification tasks, we extend the analysis of information flow to generation tasks by quantifying the mutual information between hidden states and the next token. This enables us to understand how generalization and memorization dynamics evolve for next-token generation setting during training from an information-theoretic perspective.

3 INFO RIDGE: INFORMATION ESTIMATION FRAMEWORK

We propose InfoRidge, an information-theoretic framework that uses mutual information to quantify how predictive information propagates through transformers layers during training in NLG.

Motivating Insight. Prior work has shown that internal representations in deep neural networks tend to align most closely with the true data distribution at an intermediate layer (He et al., 2024). By employing the Wasserstein distance (Villani et al., 2008), this alignment is shown to reach a minimum at a specific depth—referred to as the *generalization funnel layer*. At this point, the *Min Wasserstein Generalization Bound* (He et al., 2024) ensures that the upper bound on the gener-

alization gap—defined as the expected difference between the population and empirical risks—is minimized. This highlights the critical role of intermediate layers in supporting generalization.

Research Question. Despite the insight from prior studies of deep neural networks in classification, it remains unclear whether this generalizes to *Transformer-based language models in natural language generation (NLG)*. This motivates our central question: **In NLG, how does information evolve across layers during training, and how are different layers of the network functionally organized to support generalization versus memorization?**

Hypothesis. Building on the insight, we hypothesize that there exists a specific intermediate transformer layer that encodes the most generalizable representations for next-token prediction, characterized by maximal mutual information with the target label.

Hypothesis: Generalization Ridge

There exists an intermediate layer $\ell^* \in \{1, \dots, L\}$ such that the mutual information between the hidden state and the target label peaks at that layer:

$$\ell^* = \arg \max_{\ell} I(Z_{\ell}; Y).$$

We refer to this layer as the **generalization ridge**. This ridge layer aligns most strongly with generalizable features and serve as robust predictors under distribution shift, whereas later layers increasingly specialize in memorization.

InfoRidge Overview. To empirically investigate this hypothesis, we propose InfoRidge, an information estimation framework, that characterizes how predictive information evolves across transformer layers. Specifically, we estimate two key quantities:

- **Predictive Information** $I(Z_{\ell}; Y)$: the mutual information between the hidden state at layer ℓ and the target token. This quantity measures how much information about the true next token is contained in the layer’s full representation. A high value indicates that the layer encodes a strong and direct signal relevant to the prediction task.
- **Incremental Information Gain** $I(\Delta Z_{\ell}; Y)$: the information introduced by the residual transformation at layer ℓ , where $\Delta Z_{\ell} = Z_{\ell} - Z_{\ell-1}$. This captures the additional predictive signal gained through the residual transformation at layer ℓ , isolating how much new task-relevant information is introduced on top of the previous layer’s representation.

Together, these metrics allow us to track both the accumulation and transformation of task-relevant information throughout the network.

Notation and Setup. We consider a transformer model with L residual blocks. Given an input sequence $x_{1:T}$ of length T , $z_i^{(\ell)} \in \mathbb{R}^d$ denotes the hidden state at the last token position of the i th input sequence in layer ℓ , for $\ell = 1, \dots, L$. For next-token prediction, the ground-truth label is denoted by $y_i \in \mathbb{R}^d$, corresponding to the embedding of the true next token from the vocabulary \mathcal{V} . The residual transformation introduced at layer ℓ is defined as $\delta z_i^{(\ell)} = z_i^{(\ell)} - z_i^{(\ell-1)}$.

Across a batch of N sequences, we collect the representations:

$$Z_{\ell} = \{z_i^{(\ell)}\}_{i=1}^N, \quad Y = \{y_i\}_{i=1}^N, \quad \Delta Z_{\ell} = \{\delta z_i^{(\ell)}\}_{i=1}^N,$$

where all vectors are ℓ_2 -normalized.

Computational Flow Overview. Figure 1 illustrates the workflow used to extract intermediate representations for information analysis. In the first forward pass, a batch of N input sequences $x_{1:T}$ is fed into the transformer to obtain hidden states at each layer. From these, we extract the final-token representations Z_{ℓ} and compute the residual changes ΔZ_{ℓ} by differencing consecutive layer outputs. In the second forward pass, each input is concatenated with its ground-truth next token y , and we extract the corresponding label embedding Y from the output of the embedding

layer. These representations are then used to compute two information-theoretic quantities: the *Predictive Information* $I(Z_\ell; Y)$, and the *Incremental Information Gain* $I(\Delta Z_\ell; Y)$. We estimate both $I(Z_\ell; Y)$ and $I(\Delta Z_\ell; Y)$ using Equation 1 and 2, detailed below.

Matrix-Based Mutual Information. We apply the matrix-based framework (Giraldo et al., 2014) to estimate mutual information. Let \mathcal{U} be a random variable, from which we draw a set of vectors $U = \{\mathbf{u}_i\}_{i=1}^N \subset \mathbb{R}^d$. A positive-definite Gram matrix $G_U \in \mathbb{R}^{N \times N}$ is computed using a Gaussian kernel κ with bandwidth set to 1 and the matrix is then trace-normalized to satisfy $\text{tr}(G_U) = 1$. The matrix-based Rényi entropy (with order $\alpha = 1$) is then given by:

$$H(\mathcal{U}) \approx H(U) = -\text{tr}(G_U \log G_U). \quad (1)$$

Specifically, G_U is constructed with entries $(G_U)_{ij} = \exp\left(-\frac{\|\mathbf{u}_i - \mathbf{u}_j\|^2}{2\sigma^2}\right)$ and then trace-normalized.

Let G_U and G_V be the trace-normalized Gram matrices for two random variables \mathcal{U} and \mathcal{V} , respectively. The mutual information between them is computed as:

$$I(\mathcal{U}; \mathcal{V}) \approx I(G_U; G_V) = H(G_U) + H(G_V) - H(G_U \circ G_V), \quad (2)$$

where “ \circ ” denotes the Hadamard (elementwise) product. Mathematical details are in Appendix A.

4 EXPERIMENTAL SETUP

Models. We evaluate four models: GPT-2 SMALL (117M) (Radford et al., 2019), GPT-2 MEDIUM (345M) (Radford et al., 2019), QWEN-2.5 0.5B (Yang et al., 2024), and LLAMA 3.1 8B (Meta AI, 2024). All models are fine-tuned on NLG tasks. Each model shares weights between the input token embedding and the output language modeling head.

Datasets. We assess model behavior across three tasks casted into NLG problems: CLUTRR (Sinha et al., 2019), a relational reasoning benchmark; ECQA (Aggarwal et al., 2021), a commonsense QA benchmark; and Synthetic Arithmetic, a controlled dataset designed to disentangle task-relevant signal from noise. Dataset and implementation details are in Appendix B and C.

Synthetic Arithmetic Dataset Construction. We construct a synthetic dataset to separate signal learning from noise memorization. Each input is a sequence of 10 elements, where the signal follows an arithmetic progression modulo K , computed as $s_t = (s_0 + t \cdot d) \bmod K$ with $s_0 \in [0, K-1]$ and $d \in [1, K-1]$. Each element takes the form $S\{\text{signal}\}_N\{\text{noise}\}$, where noise is sampled from $\mathcal{U}_{\text{int}}(0, \text{noise.range}-1)$ (\mathcal{U}_{int} denotes the uniform distribution). The model is trained to predict the signal value of the final (10th) element using the preceding elements as input context. For example, with $K = 5$, $s_0 = 1$, and $d = 2$, a sample input might be $S1_N42 \ S3_N77 \dots S2_N37$, with the target signal being 4. By varying K , we can induce structured distribution shifts.

5 GENERALIZATION RIDGE: LAYER-WISE MUTUAL INFORMATION TRAINING DYNAMICS

Understanding how layers encode task-relevant information is key to uncovering the internal mechanisms that support generalization in deep language models. In this section, we trace the evolution of two complementary forms of mutual information—*Predictive Information* and *Incremental Information Gain*—across transformer depth and training time, revealing a consistent structure in information flow and highlighting the generalization–memorization trade-off.

5.1 PREDICTIVE INFORMATION: INFORMATION PEAKS AT INTERMEDIATE LAYERS

We investigate how *predictive information*—defined as the mutual information between hidden representations and target labels—evolves across the depth of transformer models. Specifically, for each layer ℓ , we compute the matrix-based mutual information $I(Z_\ell; Y)$ between the hidden state Z_ℓ and the next-token ground truth Y . This quantity measures how much task-relevant signal is retained in the representation as it propagates through the network. By tracing $I(Z_\ell; Y)$ across layers, we obtain a layer-wise trajectory of information flow, which reveals not only where predictive content is preserved but also how it is transformed or diminished as the model processes.

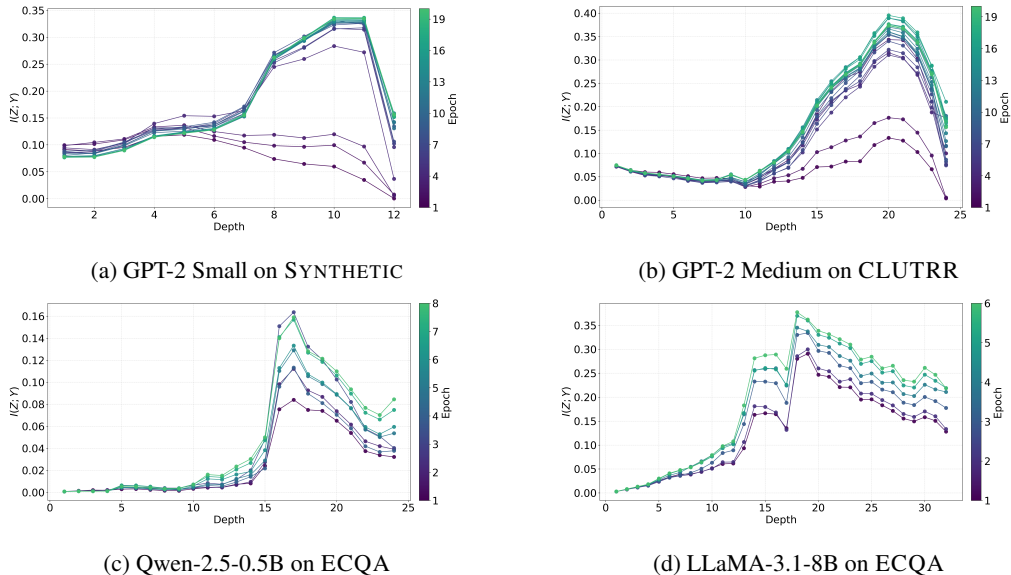


Figure 2: Evolution of predictive information $I(Z_\ell; Y)$, with lighter curves indicating later epochs. Each curve exhibits a three-phase trend: early layers rise, mid layers peak, and late layers decline.

Figure 2 tracks the trajectory of the predictive information $I(Z_\ell; Y)$ between the hidden representation at depth ℓ and the target label Y throughout training, while Table 1 reports the downstream accuracy obtained when we early exit after a given layer.¹ Additional results are in Appendix E.

Three-phase information dynamics. Across models and tasks, predictive information curves exhibit a consistent *three-phase* pattern:

Progressive Accrual (early layers). In the initial layers, $I(Z_\ell; Y)$ gradually increases, corresponding to basic feature extraction without substantial task-level comprehension. This aligns with the near-zero accuracy observed in Table 1 for these layers.

Information Peak (intermediate layers). $I(Z_\ell; Y)$ continues to rise through the mid-to-upper layer, typically peaking before the final few blocks. For the GPT-2 Small on Synthetic Arithmetic dataset, the peak reaches $I \approx 0.33$ in layers 10-11, coinciding with a jump from $\approx 0\%$ to 73% ID accuracy and 57% OOD accuracy. These layers appear to play a critical role in synthesizing abstract features that are essential for generalization.

Representational Compression (final layers). Beyond the peak, $I(Z_\ell; Y)$ decreases, even as in-distribution accuracy approaches 100%. The simultaneous drop in OOD accuracy indicates that the final layers tend to memorize training patterns, sacrificing generalization ability.

Table 1: Information Dynamics and Layer-wise Performance (GPT-2-S, Synthetic). OOD performance declines beyond the generalization ridge.

Layer	I(Z; Y)	Test Accuracy (%)		
		All	In-Dist.	Out-Dist.
Layer 1	0.0782	0.00	0.00	0.00
Layer 2	0.0776	0.00	0.00	0.00
Layer 3	0.0907	0.00	0.00	0.00
Layer 4	0.1156	0.00	0.00	0.00
Layer 5	0.1222	0.00	0.00	0.00
Layer 6	0.1275	0.00	0.00	0.00
Layer 7	0.1552	0.75	0.00	1.50
Layer 8	0.2594	19.45	0.00	40.70
Layer 9	0.2937	20.60	0.60	42.00
Layer 10	0.3295	64.25	72.90	56.90
Layer 11	0.3296	71.65	100.00	42.90
Layer 12	0.1501	70.45	100.00	41.40

¹The in distribution split is generated with $K_{id}=13$; out of distribution splits use a uniformly-sampled $K_{ood} \in \{5, \dots, 25\} \setminus \{13\}$.

Notably, this three-phase progression emerges consistently across both GPT-2 Small and GPT-2 Medium, indicating that the observed information dynamics are robust to architectural scale within the same model family.

Generalization Ridge: Memorization-Generalization Trade-off. The pronounced “information funnel” around intermediate layers reflects a key trade-off between generalization and memorization, which we term the “**generalization ridge**”. These layers maximize task-relevant information for generalization, while deeper layers increasingly compress and specialize representations, enhancing in-distribution memorization but reducing robustness. This positions intermediate layers as critical control points for managing this trade-off.

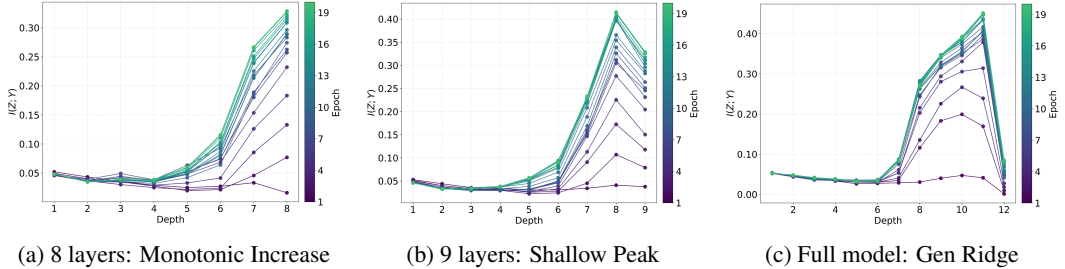


Figure 3: Truncating GPT-2 to 8 layers removes the MI peak; 9-layer variants begin to exhibit a shallow peak, and the full 12-layer model shows a pronounced decline.

Generalization Ridge Emerges Beyond a Depth Threshold We empirically vary the depth of GPT-2 Small models fine-tuned on the CLUTRR dataset to examine how model capacity shapes information dynamics, shown in Figure 3. When the model is truncated to 8 layers, $I(Z; Y)$ increases monotonically—indicating insufficient capacity to develop an information peak. Upon increasing the depth to 9 layers, a shallow peak emerges, signifying the threshold at which the model begins to distinguish generalized features from memorized signals. The full 12-layer model exhibits a clear peak followed by a decline, confirming that the generalization ridge emerges only beyond a certain capacity threshold. These results underscore the role of architectural depth in information dynamics and sufficient capacity is required for the generalization ridge to emerge.

Overfitting Adds Memorization in Final Layers

To probe overfitting dynamics, we intentionally fine-tuned the model beyond the optimal point. In Figure 4, we observe that the Predictive Information $I(Z_\ell; Y)$ rises again in the final layers—departing from the typical compression phase expected at this stage. Before overfitting, the top layers largely behave as pretrained decoders, focusing on surface-level patterns such as token co-occurrence, syntactic templates, or corpus biases, which are not strongly aligned with the task label—hence their initially low $I(Z_\ell; Y)$. After overfitting, however, the later-layer rise reflects a shift toward memorization, where the model begins to encode superficial shortcuts or redundant label-specific noise rather than useful task information.

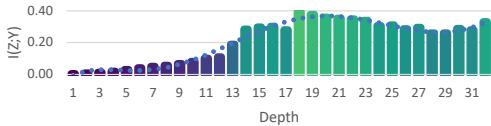


Figure 4: $I(Z_\ell; Y)$ rises in final layers during overfitting (LLaMA, ECQA).

Semantically Important Attention Peaks Where Information Peaks This discussion aims to provide an intuitive illustration of our generalization ridge hypothesis, highlighting how attention to task-relevant signal tokens shifts across layers (the generalizable information). Specifically, we computed average signal attention across layers, identified the layer with peak signal attention, and compared it to final-layer signal and last-token attention, results are in Table 2. Signal tokens are defined as task-relevant tokens that the model must focus on to solve the task—for the synthetic dataset, these are tokens that appear after the character ‘S’; for CLUTRR, kinship-related entities; and for ECQA, the token corresponding to the correct answer option. This allows us to quantify where in the network attention to semantically important information is concentrated. Our findings

show a pattern that supports our hypothesis: (1) Mid-to-late layers peak in signal attention, coinciding with the predictive information ridge (Figure 2), indicating where generalizable representations are strongest. (2) Final layers show reduced attention to signal tokens, suggesting a shift toward memorization to specific data point rather than predictive information abstraction. For example, in Qwen-2.5-0.5B on ECQA, signal attention peaks at Layer 17 (0.2458) but drops to 0.0066 in the final layer, where last-token attention dominates (0.1697). Additional results are in Appendix F.

Table 2: Average attention statistics: (1) average attention scores over all tokens, (2) average attention to signal tokens, (3) the maximum signal attention and its corresponding layer, (4) signal token attention in the final layer and (5) last token attention in the final layer.

Model	Dataset	Avg. Attn (All)	Avg. Attn (Signal)	Layer w/ Highest Avg. Signal	Final Avg. Signal	Final Avg. Last
GPT-2 Small	Synthetic	0.0227	0.0483	10 (0.0758)	0.0573	0.0400
GPT-2 Medium	CLUTRR	0.0086	0.0155	19 (0.0453)	0.0147	0.0889
Qwen-2.5-0.5B	ECQA	0.0225	0.0257	17 (0.2458)	0.0066	0.1697
LLaMA-3.1-8B	ECQA	0.0220	0.0379	21 (0.1276)	0.0168	0.3904

*We remove the first token attention score to mitigate attention sink effects.

5.2 INCREMENTAL INFORMATION GAIN: INFORMATION CONCENTRATES AT INTERMEDIATE LAYERS

To understand how information accumulates across the network, we compute *Incremental Information Gain* ($I(\Delta Z_\ell; Y)$)—the mutual information between each residual transition and the target label embedding. As shown in Figure 5, the resulting layer-wise gains reveal that intermediate layers yield the highest information increases. This concentration of information gain further underscores their central role in encoding those task-relevant features that are essential for supporting generalization. For additional illustration, a detailed case study that decodes Δz via the LM head is provided in Appendix G, highlighting fine-grained token-level shifts and variations observed across layers. The Incremental Information Gain analysis reveals a clear pattern: middle transformer blocks are key to encoding generalizable task-relevant information, thereby forming a *generalization ridge*. Conversely, later layers contribute little additional predictive signal, and in some cases, actively reduce alignment with the target embeddings. This diminishing contribution in later layers may suggest a shift from general reasoning to memorization of training-specific patterns. This trend underscores a fundamental trade-off in transformer training dynamics.

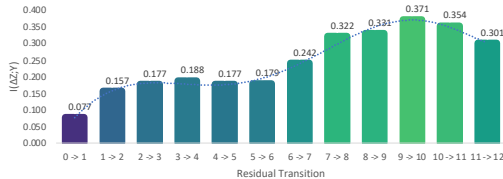


Figure 5: Middle blocks are key to encoding generalizable information (GPT-2-S, Synthetic).

6 RESIDUAL SCALING DYNAMICS VIA LEARNABLE β COEFFICIENTS

To deepen our understanding of the Generalization Ridge hypothesis, we examine how modulating the contribution of individual transformer blocks affects information flow, and propose a corollary that links layer-wise contribution to generalization performance under distribution shift.

Corollary (Residual Scaling). *Post-peak residual blocks (i.e., layers beyond the generalization ridge) may encode memorized signals. Suppressing these layers’ contribution via learned residual scaling improves out-of-distribution generalization, while amplifying them degrades it.*

We introduce a *residual scaling mechanism* with learnable scalar coefficient parameters (Algorithm 1), inspired by prior work on adaptive residual modulation (Liu et al., 2019a; Menghani et al., 2024). Transformer architectures inherently employ residual connections to iteratively refine representations. To isolate and quantify the contribution of each transformer block, we scale these residual connections with layer-specific scaling factors $\beta_\ell \in \mathbb{R}_{\geq 0}$, with definition below. Each β_ℓ controls the strength of the residual contribution from layer ℓ , enabling the model to adaptively emphasize or suppress specific blocks:

$$z^{(\ell)} = z^{(\ell-1)} + \beta_\ell \cdot \text{block}^{(\ell)}(z^{(\ell-1)}), \quad \beta_\ell \in \mathbb{R}_{\geq 0}.$$

Definition (Residual Scaling Coefficient). β_ℓ is a learnable scalar parameter associated with transformer layer ℓ , which modulates the contribution of that layer’s residual output to the model’s forward pass.

Algorithm 1 Residual Scaling: Probing the Contribution of Transformer Blocks to the Generalization–Memorization Trade-off.

Require: Pretrained Transformer with L layers, dataset \mathcal{D} , learning rate η

- 1: Initialize $\beta_1, \dots, \beta_L \leftarrow 1.0$ (trainable); freeze other weights
- 2: **for** each training step **do**
- 3: Sample batch $(x, y) \sim \mathcal{D}$
- 4: $z^{(0)} \leftarrow \text{Embedding}(x)$
- 5: **for** $\ell = 1$ to L **do**
- 6: $r^{(\ell)} \leftarrow \text{block}^{(\ell)}(z^{(\ell-1)})$
- 7: $z^{(\ell)} \leftarrow z^{(\ell-1)} + \beta_\ell \cdot r^{(\ell)}$
- 8: **end for**
- 9: Compute loss $\mathcal{L}(z^{(L)}, y)$
- 10: Update β_1, \dots, β_L using gradient descent
- 11: **end for**

We freeze model weights and optimize only the residual scaling coefficient parameters β_ℓ , which are initialized to 1. These scalars are trained separately on the (a) in-distribution (ID) split and (b) out-of-distribution (OOD) split. Since no other parameters are updated, the learned β_ℓ serve as a direct diagnostic of the extent to which each layer should be amplified or attenuated to suit the data regime, revealing which layers remain stable across regimes and which adapt strongly to distributional shifts.

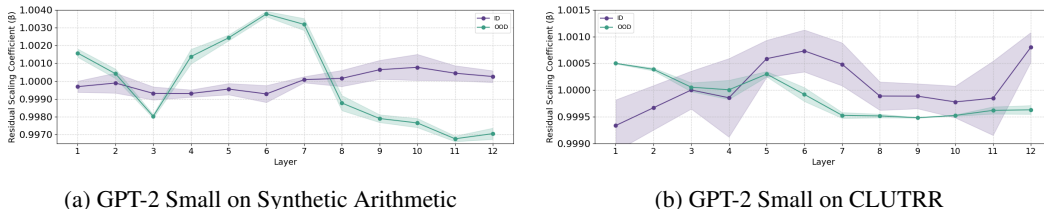


Figure 6: Residual scaling coefficients β_ℓ across all transformer layers. ID training emphasizes later layers, while OOD training has lower final layer weight. Curve shows the mean across 5 independent run, and the shaded region denotes 1- σ error bar.

As shown in Figure 6, optimizing the residual scaling coefficient parameters on in-distribution data assigns relatively higher residual weights to the final transformer layers, indicating that in-distribution performance benefits from increased reliance on late-layer residual contributions. This observation suggests that these deeper layers capture refinements that are closely tied to the training distribution. In contrast, under out-of-distribution (OOD) settings, the learned coefficients systematically have relative lower contribution of the final layers compared to the ID settings, revealing that improved generalization is associated with downweighting late-stage residual signals. More results are in Appendix E. This pattern supports the interpretation that late-layer residuals become increasingly specialized in memorized patterns tied to the training distribution. Together, these findings provide empirical support for the generalization ridge hypothesis, demonstrating that information flow in transformers reflects a trade-off between generalizable signals and memorized, distribution-specific features.

7 CONCLUSION

We introduce InfoRidge, an information-theoretic framework designed to trace and quantify how information evolves across layers in transformer-based language models for natural language generation. By estimating both predictive information and incremental information gain, we systematically characterize the layerwise dynamics of information flow, offering a principled view of how

signals are refined, amplified, or diminished as they propagate through the network. Our findings reveal a consistent *generalization ridge* emerging in intermediate layers, where mutual information between the hidden representation and the target label reaches its peak before gradually declining. This phenomenon reflects a fundamental trade-off between generalization and memorization as information flows deeper into the model. Residual scaling experiments further corroborate this interpretation, demonstrating the functional specialization of different layers. Taken together, these findings position InfoRidge as a comprehensive framework for diagnosing how language models internally manage information during natural language generation, while also revealing the structural mechanisms that govern the balance between generalization and memorization in transformer architectures.

Ethics Statement. This work adheres to the Code of Ethics. Our experiments use only open-source models and publicly available datasets under their respective open licenses, with no involvement of human subjects or sensitive data. We identify no foreseeable ethical risks.

Reproducibility Statement. We ensure reproducibility by providing experimental and implementation details in Section 4 and Appendices B–C. Full results with statistical significance are in Appendix E, and anonymous source code is included as supplementary material.

REFERENCES

- Shourya Aggarwal, Divyanshu Mandowara, Vishwajeet Agrawal, Dinesh Khandelwal, Parag Singla, and Dinesh Garg. Explanations for commonsenseqa: New dataset and models. In *Proceedings of the 59th Annual Meeting of the Association for Computational Linguistics and the 11th International Joint Conference on Natural Language Processing (Volume 1: Long Papers)*, pp. 3050–3065, 2021.
- Kyra Ahrens, Hans Hergen Lehmann, Jae Hee Lee, and Stefan Wermter. Read between the layers: Leveraging multi-layer representations for rehearsal-free continual learning with pre-trained models. *arXiv preprint arXiv:2312.08888*, 2023.
- Guillaume Alain and Yoshua Bengio. Understanding intermediate layers using linear classifier probes. *arXiv preprint arXiv:1610.01644*, 2016.
- Atsushi Ando, Ryo Masumura, Akihiko Takashima, Satoshi Suzuki, Naoki Makishima, Keita Suzuki, Takafumi Moriya, Takanori Ashihara, and Hiroshi Sato. On the use of modality-specific large-scale pre-trained encoders for multimodal sentiment analysis. In *2022 IEEE Spoken Language Technology Workshop (SLT)*, pp. 739–746. IEEE, 2023.
- Alessio Ansuni, Alessandro Laio, Jakob H Macke, and Davide Zoccolan. Intrinsic dimension of data representations in deep neural networks. *Advances in Neural Information Processing Systems*, 32, 2019.
- Guy Dar, Mor Geva, Ankit Gupta, and Jonathan Berant. Analyzing transformers in embedding space. *arXiv preprint arXiv:2209.02535*, 2022.
- Chunyuan Deng, Ruidi Chang, and Hanjie Chen. Learning distribution-wise control in representation space for language models. *arXiv preprint arXiv:2506.06686*, 2025.
- Chenhe Dong, Yinghui Li, Haifan Gong, Miaoxin Chen, Junxin Li, Ying Shen, and Min Yang. A survey of natural language generation. *ACM Computing Surveys*, 55(8):1–38, 2022.
- Siqi Fan, Xin Jiang, Xiang Li, Xuying Meng, Peng Han, Shuo Shang, Aixin Sun, Yequan Wang, and Zhongyuan Wang. Not all layers of llms are necessary during inference. *arXiv preprint arXiv:2403.02181*, 2024.
- Luis Gonzalo Sanchez Giraldo, Murali Rao, and Jose C Principe. Measures of entropy from data using infinitely divisible kernels. *IEEE Transactions on Information Theory*, 61(1):535–548, 2014.
- Ziv Goldfeld. Estimating information flow in deep neural networks. In *International Conference on Machine Learning*, 2019.

- Adi Haviv, Ido Cohen, Jacob Gidron, Roei Schuster, Yoav Goldberg, and Mor Geva. Understanding transformer memorization recall through idioms. *arXiv preprint arXiv:2210.03588*, 2022.
- Haiyun He, Christina Lee Yu, and Ziv Goldfeld. Information-theoretic generalization bounds for deep neural networks. *arXiv preprint arXiv:2404.03176*, 2024.
- Karl Moritz Hermann, Tomas Kocisky, Edward Grefenstette, Lasse Espeholt, Will Kay, Mustafa Suleyman, and Phil Blunsom. Teaching machines to read and comprehend. In C. Cortes, N. Lawrence, D. Lee, M. Sugiyama, and R. Garnett (eds.), *Advances in Neural Information Processing Systems*, volume 28. Curran Associates, Inc., 2015. URL https://proceedings.neurips.cc/paper_files/paper/2015/file/afdec7005cc9f14302cd0474fd0f3c96-Paper.pdf.
- Neil Houlsby, Andrei Giurgiu, Stanislaw Jastrzebski, Bruna Morrone, Quentin De Laroussilhe, Andrea Gesmundo, Mona Attariyan, and Sylvain Gelly. Parameter-efficient transfer learning for nlp. In *International conference on machine learning*, pp. 2790–2799. PMLR, 2019.
- Jing Huang, Zhengxuan Wu, Christopher Potts, Mor Geva, and Atticus Geiger. Ravel: Evaluating interpretability methods on disentangling language model representations. *arXiv preprint arXiv:2402.17700*, 2024.
- Mingyu Jin, Qinkai Yu, Jingyuan Huang, Qingcheng Zeng, Zhenting Wang, Wenye Hua, Haiyan Zhao, Kai Mei, Yanda Meng, Kaize Ding, et al. Exploring concept depth: How large language models acquire knowledge and concept at different layers? *arXiv preprint arXiv:2404.07066*, 2024.
- Tanishq Kumar, Blake Bordelon, Samuel J Gershman, and Cengiz Pehlevan. Grokking as the transition from lazy to rich training dynamics. In *The twelfth international conference on learning representations*, 2023.
- Fenglin Liu, Meng Gao, Yuanxin Liu, and Kai Lei. Self-adaptive scaling for learnable residual structure. In *Proceedings of the 23rd Conference on Computational Natural Language Learning (CoNLL)*, pp. 862–870, 2019a.
- Nelson F Liu, Matt Gardner, Yonatan Belinkov, Matthew E Peters, and Noah A Smith. Linguistic knowledge and transferability of contextual representations. In *Proceedings of NAACL-HLT*, pp. 1073–1094, 2019b.
- Kevin Meng, David Bau, Alex Andonian, and Yonatan Belinkov. Locating and editing factual associations in gpt. *Advances in neural information processing systems*, 35:17359–17372, 2022.
- Gaurav Menghani, Ravi Kumar, and Sanjiv Kumar. Laurel: Learned augmented residual layer. *arXiv preprint arXiv:2411.07501*, 2024.
- Amil Merchant, Elahe Rahimtoroghi, Ellie Pavlick, and Ian Tenney. What happens to bert embeddings during fine-tuning? *arXiv preprint arXiv:2004.14448*, 2020.
- Meta AI. Meta llama 3.1 8b. <https://huggingface.co/meta-llama/Llama-3.1-8B>, 2024. Accessed: 2025-05-12.
- Alec Radford, Jeff Wu, Rewon Child, David Luan, Dario Amodei, and Ilya Sutskever. Language models are unsupervised multitask learners. 2019.
- Abigail See, Peter J. Liu, and Christopher D. Manning. Get to the point: Summarization with pointer-generator networks. In *Proceedings of the 55th Annual Meeting of the Association for Computational Linguistics (Volume 1: Long Papers)*, pp. 1073–1083, Vancouver, Canada, July 2017. Association for Computational Linguistics. doi: 10.18653/v1/P17-1099. URL <https://www.aclweb.org/anthology/P17-1099>.
- Ravid Shwartz-Ziv and Naftali Tishby. Opening the black box of deep neural networks via information. *arXiv preprint arXiv:1703.00810*, 2017.

- Koustuv Sinha, Shagun Sodhani, Jin Dong, Joelle Pineau, and William L. Hamilton. Cluttr: A diagnostic benchmark for inductive reasoning from text. *Empirical Methods of Natural Language Processing (EMNLP)*, 2019.
- Oscar Skean, Md Rifat Arefin, Dan Zhao, Niket Patel, Jalal Naghiyev, Yann LeCun, and Ravid Shwartz-Ziv. Layer by layer: Uncovering hidden representations in language models. *arXiv preprint arXiv:2502.02013*, 2025.
- Ian Tenney, Dipanjan Das, and Ellie Pavlick. Bert rediscovers the classical nlp pipeline. *arXiv preprint arXiv:1905.05950*, 2019.
- Arnas Uselis and Seong Joon Oh. Intermediate layer classifiers for ood generalization. *arXiv preprint arXiv:2504.05461*, 2025.
- Ashish Vaswani, Noam Shazeer, Niki Parmar, Jakob Uszkoreit, Llion Jones, Aidan N Gomez, Łukasz Kaiser, and Illia Polosukhin. Attention is all you need. *Advances in neural information processing systems*, 30, 2017.
- Jesse Vig and Yonatan Belinkov. Analyzing the structure of attention in a transformer language model. *arXiv preprint arXiv:1906.04284*, 2019.
- Jesse Vig, Sebastian Gehrmann, Yonatan Belinkov, Sharon Qian, Daniel Nevo, Simas Sakenis, Jason Huang, Yaron Singer, and Stuart Shieber. Causal mediation analysis for interpreting neural nlp: The case of gender bias. *arXiv preprint arXiv:2004.12265*, 2020.
- Cédric Villani et al. *Optimal transport: old and new*, volume 338. Springer, 2008.
- Elena Voita, Rico Sennrich, and Ivan Titov. The bottom-up evolution of representations in the transformer: A study with machine translation and language modeling objectives. *arXiv preprint arXiv:1909.01380*, 2019.
- Zhengxuan Wu, Atticus Geiger, Thomas Icard, Christopher Potts, and Noah Goodman. Interpretability at scale: Identifying causal mechanisms in alpaca. *Advances in neural information processing systems*, 36:78205–78226, 2023.
- Zhengxuan Wu, Aryaman Arora, Zheng Wang, Atticus Geiger, Dan Jurafsky, Christopher D Manning, and Christopher Potts. Reft: Representation finetuning for language models. *Advances in Neural Information Processing Systems*, 37:63908–63962, 2024.
- An Yang, Baosong Yang, Binyuan Hui, Bo Zheng, Bowen Yu, Chang Zhou, Chengpeng Li, Chengyuan Li, Dayiheng Liu, Fei Huang, Guanting Dong, Haoran Wei, Huan Lin, Jialong Tang, Jialin Wang, Jian Yang, Jianhong Tu, Jianwei Zhang, Jianxin Ma, Jin Xu, Jingren Zhou, Jinze Bai, Jinzheng He, Junyang Lin, Kai Dang, Keming Lu, Keqin Chen, Kexin Yang, Mei Li, Mingfeng Xue, Na Ni, Pei Zhang, Peng Wang, Ru Peng, Rui Men, Ruize Gao, Runji Lin, Shijie Wang, Shuai Bai, Sinan Tan, Tianhang Zhu, Tianhao Li, Tianyu Liu, Wenbin Ge, Xiaodong Deng, Xiaohuan Zhou, Xingzhang Ren, Xinyu Zhang, Xipin Wei, Xuancheng Ren, Yang Fan, Yang Yao, Yichang Zhang, Yu Wan, Yunfei Chu, Yuqiong Liu, Zeyu Cui, Zhenru Zhang, and Zhihao Fan. Qwen2 technical report. *arXiv preprint arXiv:2407.10671*, 2024.
- Jason Yosinski, Jeff Clune, Yoshua Bengio, and Hod Lipson. How transferable are features in deep neural networks? *Advances in neural information processing systems*, 27, 2014.
- Qinan Yu, Jack Merullo, and Ellie Pavlick. Characterizing mechanisms for factual recall in language models. *arXiv preprint arXiv:2310.15910*, 2023.

A MATHEMATICAL DETAILS FOR MATRIX-BASED INFORMATION ESTIMATION AND THEORETICAL FOUNDATIONS

We employ the matrix-based Rényi entropy [Giraldo et al. \(2014\)](#) to estimate mutual information between representations and labels, leveraging kernel Gram matrices to capture sample similarity.

A.1 MATRIX-BASED ENTROPY ESTIMATION

Let $U = \{u_i\}_{i=1}^N \subset \mathbb{R}^d$ denote ℓ_2 -normalized representations obtained from a specific transformer layer, a residual update, or the embedding of the target label. A Gaussian kernel Gram matrix $G_U \in \mathbb{R}^{N \times N}$ is constructed as: $(G_U)_{ij} = \exp\left(-\frac{\|u_i - u_j\|^2}{2\sigma^2}\right)$, with bandwidth $\sigma = 1$. The matrix is then trace-normalized to ensure $\text{tr}(G_U) = 1$.

The matrix-based Rényi entropy of order $\alpha = 1$ is defined as:

$$H(U) = -\text{tr}(G_U \log G_U).$$

This expression can be interpreted in terms of the eigenvalue spectrum $\{\lambda_k\}$ of G_U , since G_U is positive semi-definite and trace-normalized:

$$H(U) = -\sum_{k=1}^N \lambda_k \log \lambda_k.$$

The entropy thus reflects the dispersion of the eigenvalues. A more uniform spectrum (i.e., higher entropy) suggests more diversity in the representation space, while a sharply peaked spectrum (i.e., low entropy) indicates redundancy or compression.

A.2 MUTUAL INFORMATION ESTIMATION

To estimate the mutual information between two random variables U and V , we compute their Gram matrices G_U and G_V , and form the joint similarity matrix via element-wise (Hadamard) product: $G_{UV} = G_U \circ G_V$. After trace-normalization, mutual information is estimated by: $I(U; V) = H(U) + H(V) - H(U, V)$, where $H(U, V) = -\text{tr}(G_{UV} \log G_{UV})$. The eigenvalue spectrum of G_{UV} governs the joint entropy term; its shape reflects how much of the structure in U and V aligns. A more concentrated spectrum in G_{UV} relative to G_U and G_V implies stronger dependence and thus higher mutual information.

A.3 MIN WASSERSTEIN GENERALIZATION BOUND ([HE ET AL., 2024](#))

We restate the generalization bound proposed by He et al. ([He et al., 2024](#)), which characterizes generalization in terms of the Wasserstein distance between internal representations.

Suppose that the loss function $\tilde{\ell} : \mathcal{Y} \times \mathcal{Y} \rightarrow \mathbb{R}_{\geq 0}$ is ρ_0 -Lipschitz, and the activation function $\phi_\ell : \mathbb{R} \rightarrow \mathbb{R}$ is ρ_ℓ -Lipschitz for each $\ell = 1, \dots, L$. Then:

$$\text{gen}(P_{W|\mathcal{D}_n}, P_{X,Y}) \leq \min_{\ell} \frac{\rho_0}{n} \sum_{i=1}^n \mathbb{E}_W \left[\left(1 \vee \prod_{j=\ell+1}^L \rho_j \|W_j\|_{\text{op}} \right) \cdot \mathcal{W}_1(P_{T_\ell, i, Y_i|W}(\cdot|W), P_{T_\ell, Y|W}(\cdot|W)) \right] \quad (3)$$

This result shows that generalization can be tightly controlled by the Wasserstein distance ([Villani et al., 2008](#)) between representations at a specific layer—referred to the generalization funnel layer.

Connection to Our Work. The *Min Wasserstein Generalization Bound* ([He et al., 2024](#)) provides a theoretical foundation for our study by characterizing generalization in terms of distributional alignment at an intermediate layer. It motivates our analysis of information flow by suggesting that information is peaked at a specific layer—the generalization funnel. Our InfoRidge builds on this insight by quantifying predictive information across layers, and reveals that a specific intermediate layer exhibits peak mutual information and correlates with better generalization performance.

B DATASET OVERVIEW AND STATISTICS

To evaluate information flow and generalization dynamics across model layers, we conduct experiments on three datasets with varying levels of complexity and structure: CLUTRR, ECQA, and a custom-designed Synthetic Arithmetic dataset. Table B.1 summarizes key dataset statistics.

B.1 DATASET OVERVIEW

Table 3: Dataset Statistics

Dataset	#Train	Train Seq. Len	#Val	Val Seq. Len	#Test	Test Seq. Len
CLUTRR	9,074	30	2,020	29	1,146	70
ECQA	7,598	21	1,090	21	2,194	21
Synthetic Arithmetic	10,000	9	2,000	9	2,000	9

B.2 CLUTRR

CLUTRR (Compositional Language Understanding and Text-based Relational Reasoning) (Sinha et al., 2019) is a diagnostic benchmark for evaluating relational inference in language models. Each example contains a story describing family relations, and the task is to infer the missing relationship between two entities. The distribution shift stems from clause lengths that are absent in the training set but present during evaluation. We use the task split “gen_train23_test2to10”, where the model is trained on clause lengths 2 and 3 and evaluated on lengths 2 through 10.

B.3 ECQA

ECQA (Explanations for CommonsenseQA) (Aggarwal et al., 2021) is a commonsense multiple-choice question-answering dataset, where each question is accompanied by 5 answer options.

B.4 SYNTHETIC ARITHMETIC DATASET

We construct a synthetic diagnostic dataset to disentangle task-relevant signal learning from spurious noise memorization in a controlled setting. Each sample consists of a sequence of 10 symbolic elements, where the signal component follows an arithmetic progression modulo K , and the remainder of each element is independently corrupted with random noise. By varying the modulus K , we systematically control task complexity and introduce structured shifts in the data distribution.

Synthetic Arithmetic Dataset Construction. At each position t , the signal value is computed as:

$$s_t = (s_0 + t \cdot d) \bmod K, \quad \text{with } s_0 \in [0, K-1], \quad d \in [1, K-1].$$

Each element in the sequence is represented as a string of the form:

$$S\{\text{signal}\}_N\{\text{noise}\}, \quad \text{where } \text{noise} \sim \mathcal{U}_{\text{int}}(0, \text{noise_range}-1).$$

Here \mathcal{U}_{int} denotes the uniform distribution. The model is trained to predict the signal value of the final (10th) element, using the preceding elements as input context.

For example, with $K = 5$, $s_0 = 1$, and $d = 2$, a sample might look like:

S1.N42 S3.N77 S0.N18 S2.N56 S4.N90 S1.N11 S3.N65 S0.N23 S2.N37

Each element encodes both a signal (the number following S) and a noise component (the number following N). The target is 4, corresponding to the signal of the final (10th) item in the sequence.

C IMPLEMENTATION DETAILS

This appendix outlines implementation details in our experiments.

C.1 PROMPT CONSTRUCTION

All tasks are cast into a next-token generation format. The model receives a prompt and generate the next token. Below are construction strategies and examples for each dataset:

CLUTRR Each input example in CLUTRR consists of a short narrative describing a set of family relationships, along with a query involving a pair of entities. We construct prompts by concatenating the narrative and a structured natural language question derived from the query tuple. The model is trained to predict the correct relationship as the next token.

Prompt:

Story: [Alice] is [Bob]’s mother. [Bob] is [Charlie]’s father.
Query: What is the relationship between Alice and Charlie? Answer:

Target: grandmother

ECQA (Explanation-augmented Commonsense QA) Each ECQA instance consists of a multiple-choice question with five candidate answers. We format the prompt by presenting the question followed by all five options (labeled A–E), and conclude with an explicit answer query. The model is trained to predict the correct answer letter as the next token.

Prompt:

Question: What do people usually do at a birthday party?
Options:
A. Sleep
B. Celebrate
C. Cook
D. Exercise
E. Drive
Answer:

Target: B

Synthetic Arithmetic Each synthetic sample consists of a sequence of 10 symbolic elements, where each element is formatted as $S\{\text{signal}\}_N\{\text{noise}\}$. The signal values follow an arithmetic progression modulo K , and the noise values are independently sampled from a uniform distribution with a fixed range of 100. During training, the modulus K is set to 13. For evaluation, test sequences are generated using values of K from the range $[5, 26]$ excluding 13 to simulate a distribution shift. In the residual β_ℓ analysis, we use $K = 13$ for in-distribution (ID) training and $K = 17$ for out-of-distribution (OOD) training, allowing for a controlled comparison between generalization and memorization behavior. The model receives the first 9 tokens as input and is trained to predict the signal component of the 10th token.

Prompt:

S1_N42 S3_N88 S5_N20 S7_N10 S9_N65 S11_N43 S0_N99 S2_N38 S4_N77

Target: 6

This controlled format enables manipulation of distributional properties by varying the modulus K .

C.2 FINETUNING SETTINGS

We fine-tuned all layers end-to-end using AdamW (learning rate 5×10^{-6} , weight decay 0.01) with a linear schedule (warmup ratio 0.1) and early stopping on validation loss. Training converged in all settings.

C.3 INFORMATION ESTIMATION

To estimate mutual information, we subsample between 50 and 200 test examples depending on model and task to achieve a stable result.

C.4 RESIDUAL SCALING WITH LEARNABLE β_ℓ PARAMETERS

We introduce a vector of learnable scalar weights $\beta = \{\beta_1, \dots, \beta_L\}$ applied to residual connections in a frozen transformer:

$$z^{(\ell)} = z^{(\ell-1)} + \beta_\ell \cdot \text{Block}^{(\ell)}(z^{(\ell-1)}).$$

- All transformer weights are frozen; only β_ℓ parameters are trained.
- Each transformer block’s residual output is modulated by β_ℓ via forward hooks.
- β are initialized to 1 and updated using gradient descent without altering the architecture.

Training and Evaluation Settings We perform residual β_ℓ training on top of a model that has already been fine-tuned on the target dataset, keeping all previously learned weights frozen and optimizing only the β_ℓ parameters using HuggingFace’s Trainer API. We sweep over batch sizes from 4 to 32 depending on GPU memory constraints, and tune the learning rate between 5×10^{-5} and 5×10^{-6} . We train for 3–10 epochs based on model capacity and task complexity. Optimization is performed using the AdamW optimizer with a weight decay of 0.01. Evaluation is conducted by comparing the next predicted token with the next ground-truth target token.

Table 4: Performance (%) of different models across datasets.

Model	CLUTRR	Synthetic	ECQA
GPT-2 Small	30.98	71.45	—
GPT-2 Medium	34.21	68.35	—
Qwen-2.5-0.5B	31.94	83.20	57.06
LLaMA-3.1-8B	57.68	94.00	77.39

D COMPUTE AND LICENSING DETAILS

Computing Resources Experiments were conducted on an NVIDIA RTX A6000 GPU (48GB).

Model Licenses The GPT-2 Small (Radford et al., 2019) and GPT-2 Medium (Radford et al., 2019) models are released under the MIT License and are available via Hugging Face Transformers. The Qwen-2.5 0.5B (Yang et al., 2024) model is provided by Alibaba Group under the Apache 2.0 License. The LLaMA-3.1 8B (Meta AI, 2024) model is made available by Meta under a non-commercial research license and accessed via Hugging Face.

Dataset Licenses CLUTRR (Sinha et al., 2019) is released under a CC BY 4.0 license as part of EMNLP 2019. The ECQA (Aggarwal et al., 2021) dataset is also released under a CC BY 4.0 license by its authors as part of EMNLP 2021. The Synthetic Arithmetic dataset is custom-designed by the authors and does not rely on any external or licensed data sources.

All assets were used in compliance with their respective licenses, and no proprietary or restricted resources were employed in our experiments.

E FULL QUANTITATIVE RESULTS WITH CONFIDENCE ESTIMATES

To provide a comprehensive view of model behavior, we report the full experimental results for all models and datasets. This includes predictive information trends ($I(Z; Y)$), incremental information gain ($I(\Delta Z; Y)$) and residual scaling effects (β_ℓ), with statistical significance reporting.

E.1 PREDICTIVE INFORMATION

To estimate mutual information between hidden representations and target labels, we compute matrix-based mutual information following the methodology in Appendix A. We subsample between 50 and 100 test examples per experiment and report results with statistical significance based on multiple random seeds.

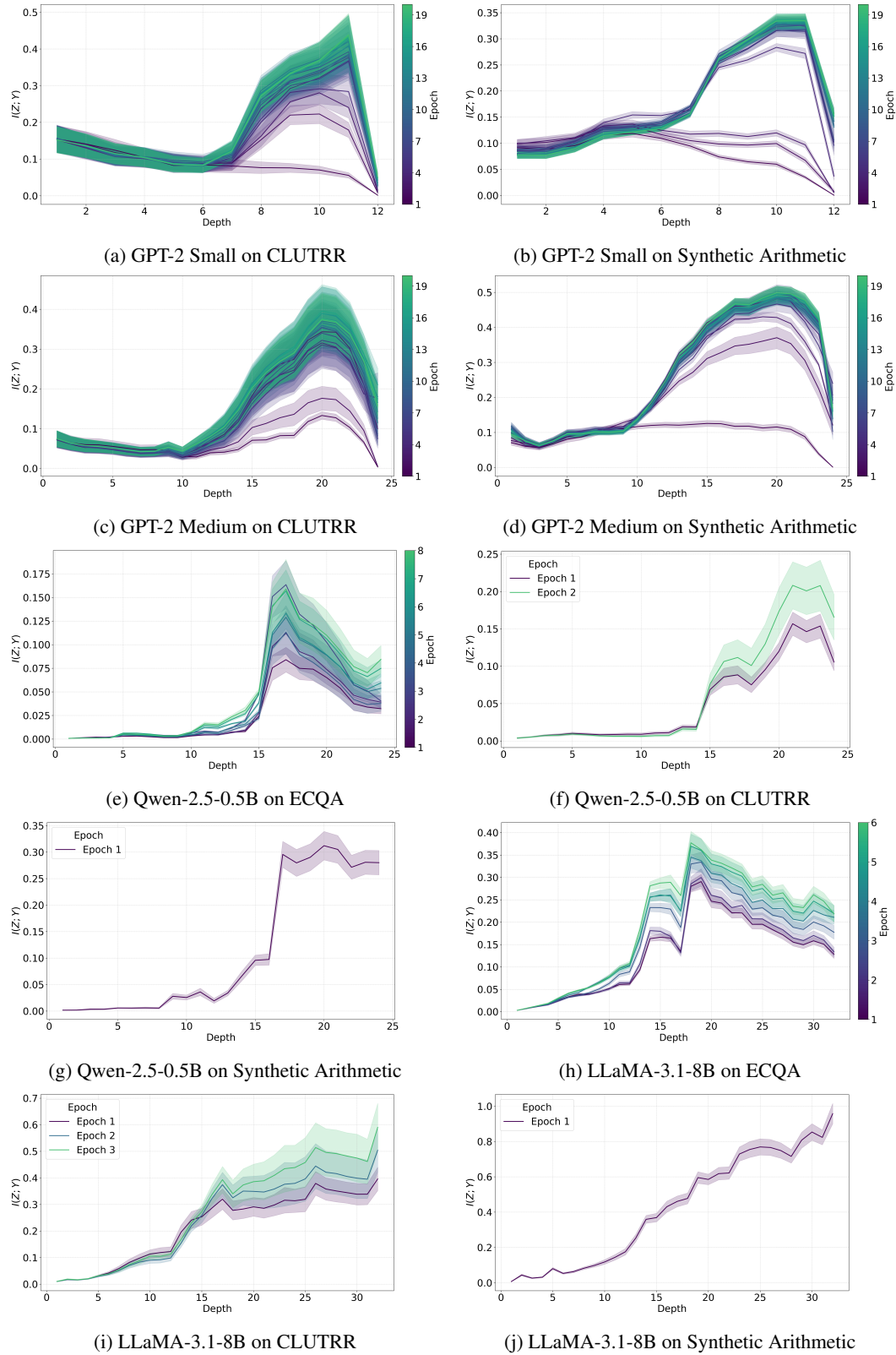


Figure 7: Predictive information $I(Z; Y)$ across different models and datasets exhibits an information peak, indicating a generalization ridge. In cases where the task is too simple relative to model capacity—such as the synthetic arithmetic task with LLaMA—this trend reflects an overfitting regime. Lighter line colors represent later training epochs. Each curve shows the mean across 5 random seeds (0, 1, 2, 3, 42), and the shaded region denotes a 2-sigma ($\sim 96\%$) confidence interval.

E.2 INCREMENTAL INFORMATION GAIN

In addition to predictive information $I(Z^{(\ell)}; Y)$, we compute the incremental information gain $I(\Delta Z^{(\ell)}; Y)$ at each layer. This quantifies the information contribution for each transformer block.

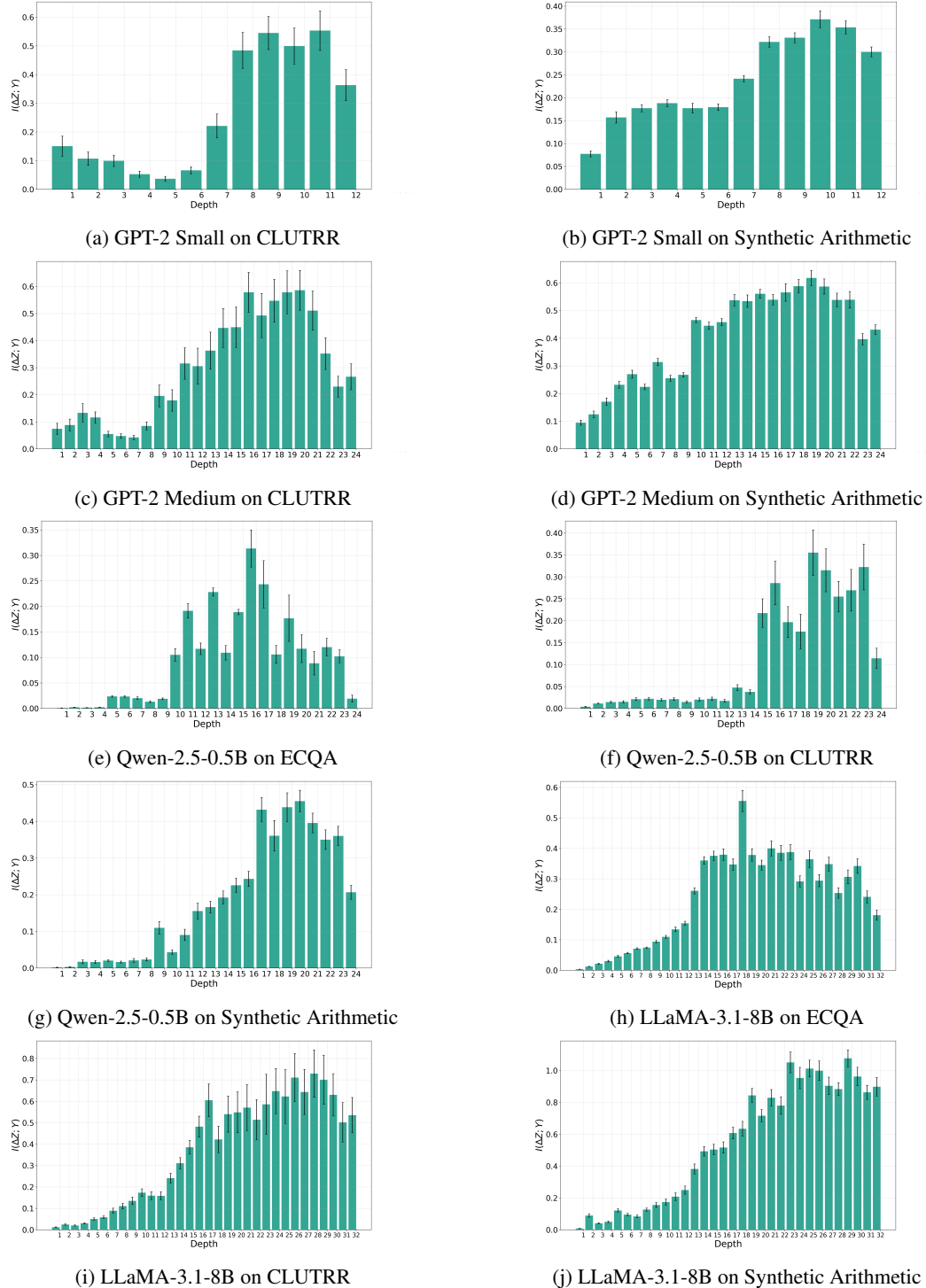


Figure 8: Incremental information gain $I(\Delta Z; Y)$ across different models and datasets with $\sim 96\%$ CI error bars. Across all models, we observe that the largest incremental information gain consistently occurs in intermediate layers—further supporting the emergence of a generalization ridge.

E.3 RESIDUAL SCALING

We introduce a *residual scaling mechanism* with learnable scalar coefficient parameters, inspired by prior work on adaptive residual modulation (Liu et al., 2019a; Menghani et al., 2024). Similar ideas of modulating internal computation have also been explored in parameter-efficient fine-tuning (PEFT) (Houlsby et al., 2019), Representation-Efficient Fine-Tuning (REFT) (Wu et al., 2024) and interpretability-driven control (Huang et al., 2024; Deng et al., 2025; Meng et al., 2022; Wu et al., 2023). We present the complete set of residual scaling results, detailing the learned β_ℓ values across all transformer layers. These values reflect the relative contribution of each layer after optimizing the residual scaling coefficients while keeping all other model parameters frozen. β_ℓ are trained on in-distribution (ID) and out-of-distribution (OOD) data. We observe that in the ID setting, later layers tend to receive higher weights, consistent with memorization behavior. In contrast, OOD training consistently has lower final layers’ weight compared to the ID settings and shifts importance toward the intermediate layers. When the task is simple relative to the model’s capability, such as LLaMA on the synthetic task, the final-layer residual coefficients are similar for ID and OOD, consistent with Figure 7. The in-distribution (ID) setting is using the training split of “gen_train23_test2to10”. Out-of-distribution (OOD) is conducted on held-out CLUTRR configurations that do not overlap with the training distribution: for GPT models we evaluate on the test split of “gen_train23_test2to10” (lengths 2 through 10), while for Qwen and LLaMA we use the test split of “rob_train_sup_23_test_all_23”, which defines a more challenging OOD setting by jointly varying both the clause length and the status of noise facts introduced into the story, given the higher modeling capacity of these models. In all cases, tasks 1.2 and 1.3 are excluded from the OOD sets, as they overlap with the training configuration and are therefore treated as in-distribution rather than out-of-distribution.

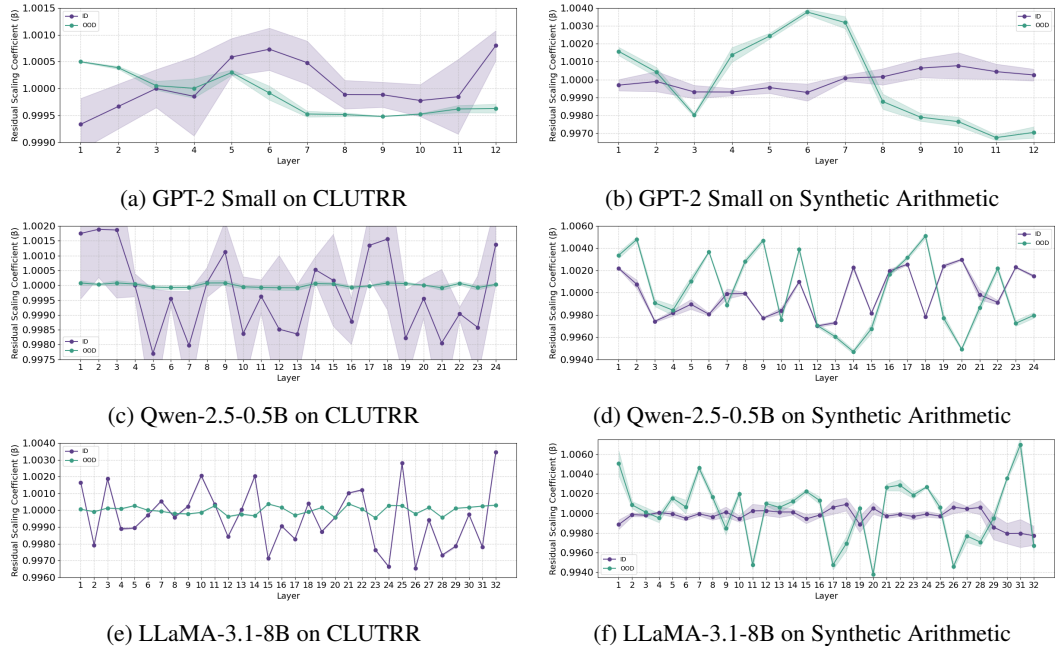


Figure 9: Residual scaling coefficients β_ℓ across all transformer layers. ID training emphasizes later layers, while OOD training has lower final layer weight. Each curve shows the mean across five random seeds (0, 1, 2, 3, 42), and the shaded region denotes 1-sigma error bar.

F ATTENTION DYNAMICS ACROSS LAYERS CASE STUDY

To verify whether generalization ridge layer indeed correspond to semantically meaningful processing, we visualize the attention patterns as a more interpretable signal of where the model focuses. As shown in Figure 10, we visualize attention maps across layers.

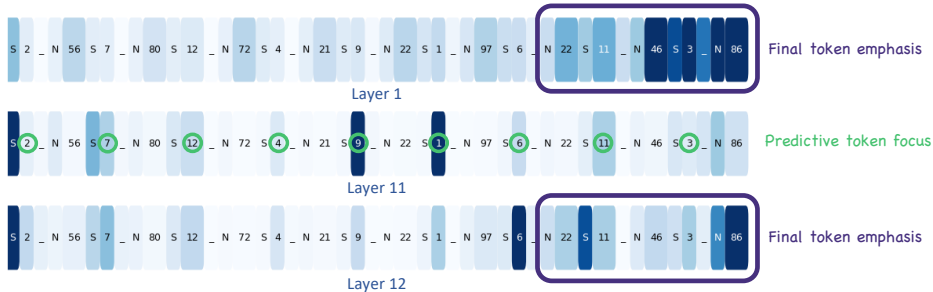


Figure 10: Attention map across layers (GPT-2 Small, Synthetic). At the generalization ridge layers, attention becomes more targeted, focusing on predictive tokens.

In early layers (e.g., Layer 1), attention is diffuse and biased toward final tokens—reflecting reliance on position rather than true predict signals.

By generalization ridge layers (e.g., Layer 11), attention becomes more targeted, concentrating on predictive tokens. This shift marks a transition from positional attention to semantically meaningful focus, suggesting that intermediate layers are increasingly capable of isolating task-relevant information from irrelevant content.

In the final layers, attention regresses toward final tokens. This reversion is aligned with the observed decline in $I(Z_\ell; Y)$. The resurgence of attention towards terminal tokens indicates a potential memorization scenario, where the model re-engages superficial positional strategies, possibly memorizing noise rather than further refining the generalized extraction of predictive signals.

This attention trajectory further supports the generalization ridge hypothesis, highlighting a trade-off between generalization and memorization in the model’s representational strategy.

G INCREMENTAL INFORMATION GAIN CASE STUDY

To further illustrate how intermediate layers contribute to generalization, we analyze the semantic content introduced by residual transitions at different depths. Specifically, we decode the residual transition δz at each layer using the language modeling (LM) head, projecting the incremental representation back into token space.

This analysis allows us to inspect the linguistic shift introduced by each transformer block in isolation, and to assess whether the changes correspond to task-relevant predictions or superficial noises.

G.1 METHODOLOGY

For a fixed input, we compute residual transitions $\delta z^{(\ell)}$ at each layer and pass them through the model’s final linear projection (LM head) followed by a softmax. We record the top predicted tokens and their probabilities, and it reflects the directional change applied by layer ℓ .

G.2 OBSERVATIONS

We decode residual transitions across layers and report the top shifted tokens by projecting $\Delta Z^{(\ell)}$ through the LM head. These shifts provide insight into how each layer modifies the model’s internal prediction trajectory.

Layer 9 \rightarrow 10: The top shifted tokens include $\mathbb{G}9$, $\mathbb{G}10$, $\mathbb{G}4$, $\mathbb{G}8$, and 8, which are all numerically aligned with the target prediction space in the synthetic arithmetic task. This indicates that the model is beginning to refine task-relevant numerical features at this depth.

Layer 10 \rightarrow 11: The shifted tokens become partially diluted, featuring punctuation and less informative symbols such as \cdot , \mathbb{G} , and \cdot , alongside occasional task-relevant entries like $\mathbb{G}12$ and $\mathbb{G}4$. This indicates a transitional phase where the model continues to refine meaningful task-relevant fea-

tures, yet begins to exhibit noise from frequent but semantically uninformative, such as punctuation, tokens.

Layer 11 \rightarrow 12: At the final layer transition, the top 5 shifted tokens become largely uninterpretable, including `Gcanaver`, `soDeliveryDate`, `enegger`, `76561`, and `ILA`. Conversely, the most negatively shifted tokens—`G4`, `G3`, `G5`, `G6`, `G1`—correspond to plausible numerical predictions that were actively suppressed. This supports the hypothesis that final layers may overwrite generalizable abstractions with memorized or noise signals.

These patterns are consistent with our mutual information analysis, which identifies intermediate layers as better semantically aligned with the prediction target—forming a ridge of generalization.

G.3 IMPLICATION

These decoding results reinforce our interpretation of the generalization ridge: intermediate layers contribute the most semantically informative updates to the model’s representation. The residual transitions thus serve as a useful lens for understanding how and where semantic meaning is introduced during forward propagation.

H ACTIVATION PATCHING EXPERIMENT

To assess which residual blocks causally support OOD prediction, we conduct a targeted activation-patching experiment. Let the model contain L residual blocks with hidden states $Z_\ell \in \mathbb{R}^d$, and let t^* denote the final context token (the last token before next-token prediction). For every OOD sequence x_{ood} , we pair it with an ID sequence x_{id} sharing the same token structure. For each depth $\ell \in \{1, \dots, L\}$, we compute two forward passes: a standard OOD pass and a patched pass in which we replace only the hidden state of token t^* at depth ℓ according to $Z_\ell(x_{\text{ood}}, t^*) \leftarrow Z_\ell(x_{\text{id}}, t^*)$. All other activations remain unchanged. Let $\text{logit}_{\text{base}}^{t^*}$ denote the logit assigned to the correct next token under the baseline OOD pass, and let $\text{logit}_{\text{patch}}^{(\ell)}$ denote the corresponding logit under layer- ℓ patching. We measure causal impact using the logit drop $\Delta_\ell = \text{logit}_{\text{base}}^{t^*} - \text{logit}_{\text{patch}}^{(\ell)}$, where a positive value indicates that depth ℓ provides information necessary for correct OOD prediction.

Table 5 reports the averaged logit drop for all $\ell = 1, \dots, 12$ (GPT-2 Small on Synthetic Dataset). The effects are negligible for layers 1–8, begin rising around layer 9, increase sharply at layer 10, peak at layer 11, and decline again at layer 12. This rise–peak–fall pattern closely matches the ridge structure observed in Figure 2, where $I(Z_\ell; Y)$ increases through mid-to-late depth, reaches a maximum in the ridge region, and then decreases. The activation-patching experiment therefore provides supporting causal evidence that the ridge layers identified by IndoRidge are necessary for successful OOD generalization.

Table 5: Average logit drop Δ_ℓ (baseline logit - patched logit). Larger values indicate greater causal contribution to OOD prediction.

Layer ℓ	1	2	3	4	5	6	7	8	9	10	11	12
Δ_ℓ	-0.1037	-0.1039	-0.0327	-0.5405	-5.1663	-8.3992	-5.8914	-15.0996	-3.0998	9.3148	17.2022	15.5943

I EXTENDING PREDICTIVE INFORMATION TO MULTI-TOKEN OUTPUTS

To complement our single-token analysis, we further evaluate information flow under multi-token outputs using the CNN/Daily Mail summarization dataset (1.0.0, test) (See et al., 2017; Hermann et al., 2015).

Autoregressive next-token information. We follow the model’s natural decoding process. We analyze $I(Z_\ell^{(t)}; \hat{Y}^{(t+1)})$ since there is no deterministic gold answer for each intermediate step in NLG, where for each generation step t , $Z_\ell^{(t)}$ is the hidden state of current token at layer ℓ and $\hat{Y}^{(t+1)}$ is the embedding of model’s predicted token at step $t + 1$.

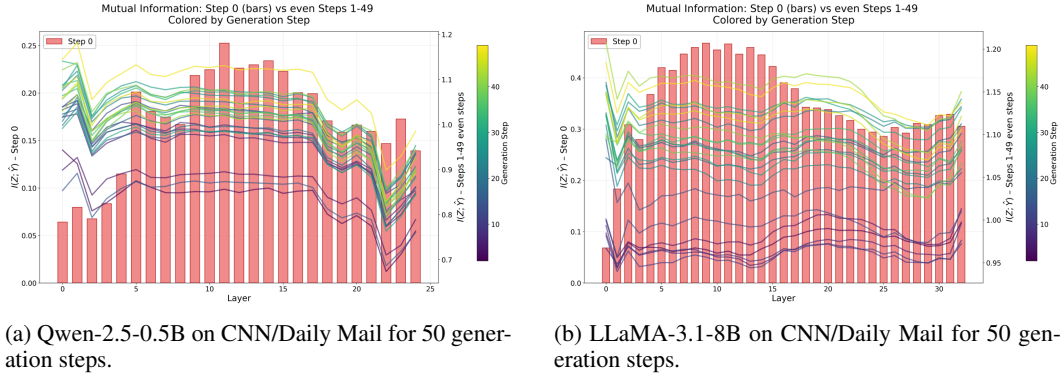


Figure 11: $I(Z_\ell^{(t)}; \hat{Y}^{(t+1)})$ across layers (x-axis) and generation steps (y-axis), where the left y-axis shows first step mutual information (bars) and the right y-axis shows mutual information for the rest steps.

Across steps, the pattern is consistent (Figure 11): information rises from early layers, peaks in the middle layers, and then declines toward top layers. This gives a clear information ridge, indicating that intermediate layers encode the most stable and task-relevant core information that supports the model’s decision-making (generalization). In particular, high $I(Z_\ell^{(t)}; \hat{Y}^{(t+1)})$ at these layers means the model’s predictive direction is most strongly determined by that layer: layers whose representations consistently constrain the next-token prediction across many contexts must encode the shared, invariant structure that the model relies on to generalize. In contrast, upper layers exhibit behavior that might be related to pretrained surface patterns from corpus such as token co-occurrence, causing the representation to drift away from this decision-relevant structure (memorization).

The first step is a notable outlier: it is the only step that conditions solely on the input prompt, and shows the sharpest and most pronounced ridge. Generating the first token requires a global transition from the prompt into the answer trajectory, which heavily engages the abstract, decision-relevant subspace in the middle layers. Crucially, this is also the point where information compression is most extreme, the model must condense all prompt-level semantics into a single initial token decision, therefore forms a substantial ridge. Once generation begins, later generation steps move into a more regular autoregressive regime, where each hidden state already contains a compressed summary of all previously generated content, and the continuation depends more on local context than on global restructuring. Consequently, the depth profiles become flatter and more stable across steps, although the mid-layer ridge remains visible.

Pooled-answer information. We quantify how much information each layer carries about the gold answer by computing $I(Z_\ell^{(t)}; Y^{\text{pool}})$, where Y^{pool} is a fixed target vector obtained by average-pooling the embedding-layer representations of all ground-truth answer tokens. Across models and steps (Figure 12), a consistent pattern emerges: intermediate layers are where the hidden state is most strongly aligned with the gold-answer.

Taken together, the two constructions reveal a coherent picture of depth specialization in multi-token generation. Intermediate layers are simultaneously the most informative about the model’s next-token decisions and the most aligned with the global answer. Thus, the two observed ridges are complementary projections of a single underlying phenomenon: intermediate layers concentrated most meaningful and decision-relevant information. In contrast, upper layers increasingly reflect pretrained corpus-specific surface patterns, causing the representation to drift away from this decision-relevant structure.

We also plot the mutual information comparing stopwords/punctuation against content words, showing that both stopwords/punctuation have consistently higher MI (Figure 13). These tokens are more predictable because they follow strict grammatical and structural patterns, whereas content words depend more on semantic context and therefore exhibit greater variability.

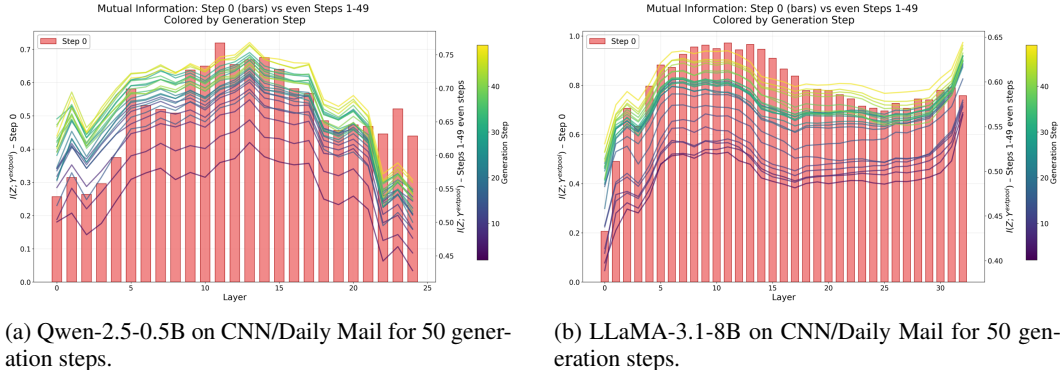


Figure 12: $I(Z_\ell^{(t)}; Y^{\text{pool}})$ across layers (x-axis) and generation steps (y-axis), where the left y-axis shows first step mutual information (bars) and the right y-axis shows mutual information for the rest steps.

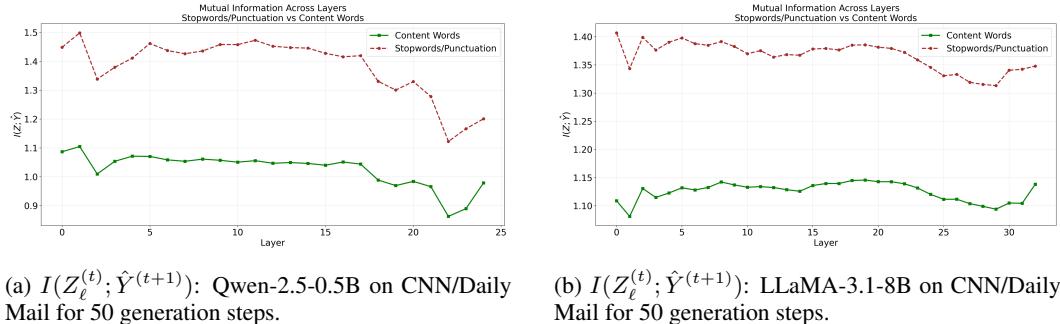


Figure 13: Mutual information comparing stopwords/punctuation against content words, showing that both stopwords/punctuation have consistently higher MI.

J NON-FINETUNED SCENARIO

Beyond fine-tuning scenarios, we also computed predictive-information $I(Z_\ell; Y)$ curves in a non-training zero-shot regime and observed the same mid-layer information peak pattern, see Figure 14.

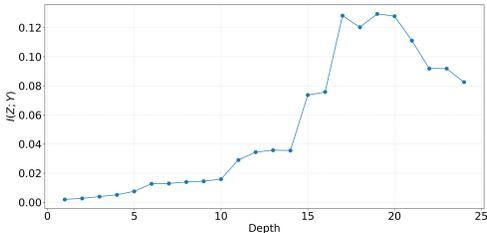
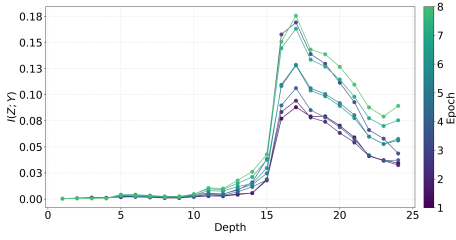


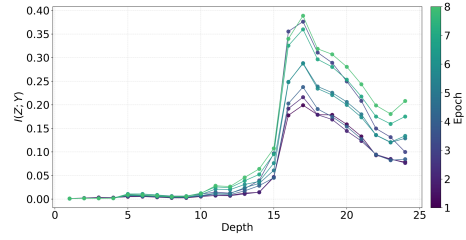
Figure 14: GSM8K on Qwen2.5-0.5B shows an intermediate-layer MI rise and late-layer decline.

K KERNEL ABLATION

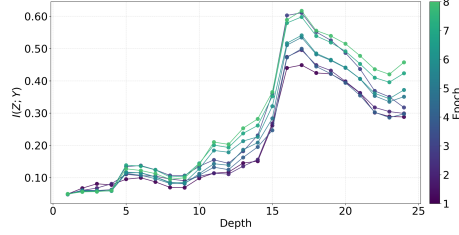
The matrix-based MI estimator requires a positive-definite Gram matrix, for which the Gaussian kernel is the standard choice. To assess robustness with respect to kernel selection, we additionally test the Laplacian and Polynomial kernels. While these kernels introduce quantitative shifts in the magnitude, the trend—including the rise–peak–decline structure and the location of the ridge—remains unchanged (Figure 15).



(a) Gaussian Kernel: Qwen-2.5-0.5B on ECQA.



(b) Polynomial Kernel: Qwen-2.5-0.5B on ECQA.



(c) Laplacian Kernel: Qwen-2.5-0.5B on ECQA.

Figure 15: Different kernel shows similar pattern.

Polynomial Kernel. Given a set of normalized representations $U = \{u_i\}_{i=1}^N$, the polynomial kernel Gram matrix is defined as

$$(G_U^{\text{poly}})_{ij} = (u_i^\top u_j + c_0)^p, \quad (4)$$

where p is the polynomial degree and c_0 is a constant bias term.

Laplacian Kernel. Given the same representation set $U = \{u_i\}_{i=1}^N$, the Laplacian kernel Gram matrix is defined as

$$(G_U^{\text{lap}})_{ij} = \exp(-\gamma \|u_i - u_j\|_1), \quad (5)$$

where $\gamma > 0$ is a kernel coefficient and $\|\cdot\|_1$ denotes the ℓ_1 distance.

L USE OF LARGE LANGUAGE MODELS.

Large language models (LLMs) were used solely as assistive tools for proofreading and improving clarity of writing.